X-Tandem: Towards Multi-hop Backscatter Communication with Commodity WiFi

Jia Zhao
Simon Fraser University
BC, Canada
zhaojiaz@sfu.ca

Wei Gong
University of Science and Technology of China, China
Simon Fraser University, Canada
weigong@ustc.edu.cn

Jiangchuan Liu
Simon Fraser University
BC, Canada
jcliu@cs.sfu.ca

ABSTRACT

Backscatter communication offers a cost- and energy-efficient means for IoT sensor data exchange. The IoT vision for ubiquitous interconnection, in practice, demands multi-hop connectivity for robust and scalable sensor networks, as well as compatibility with such prevailing wireless technologies as WiFi. Today's backscatter solutions however typically follow a single-hop paradigm, i.e., tags do not relay for each other.

This paper presents X-Tandem, a multi-hop backscatter system that works with commodity WiFi devices. For the first time, we demonstrate that sensing tags can not only work as relays for each other but also modulate their sensing data into *a single backscatter packet*, which remains a legit WiFi packet that can be decoded with any commercial WiFi NICs. We discuss the design details of X-Tandem and have built a prototype with FPGAs and off-the-shelf WiFi devices. The prototype demonstrates a two-hop implementation, achieving a throughput up to 200 bps with tag-to-tag distances up to 0.4 m and communication ranges up to 8 m. Compared to single-hop solutions, X-Tandem can improve backscatter throughput by more than 10x in challenging indoor environments with obstacles.

CCS CONCEPTS

• **Networks** → **Cyber-physical networks**; **Network architectures**; **Sensor networks**;

KEYWORDS

Backscatter; Multi-hop; WiFi; Internet-of-Things

MobiCom'18, October 29–November 2, 2018, New Delhi, India

ACM ISBN 978-1-4503-5903-0/18/10…$15.00
https://doi.org/10.1145/3241539.3241553

ACM Reference Format:
Jia Zhao, Wei Gong, and Jiangchuan Liu. 2018. X-Tandem: Towards Multi-hop Backscatter Communication with Commodity WiFi. In *MobiCom '18: 24th Annual Int'l Conf. on Mobile Computing and Networking, Oct. 29–Nov. 2, 2018, New Delhi, India.* ACM, New York, NY, USA, 15 pages. https://doi.org/10.1145/3241539.3241553

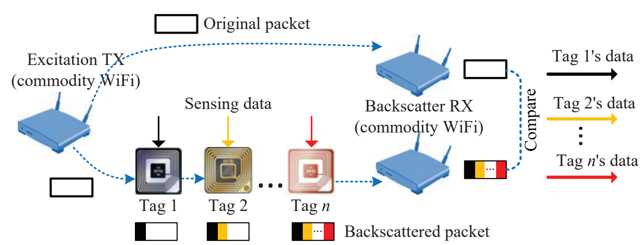

Figure 1: X-Tandem communication. Backscatter tags relay for previous hops and embed sensor data on ambient WiFi signals, being fully compatible with commodity WiFi.

1 INTRODUCTION

Internet of Things (IoT) applications connect the physical world to the digital world, providing smart control, pervasive sensing, and intelligent interaction. To achieve cost-effectiveness and ubiquitous connectivity, a fast-growing presence of IoT solutions are using such mainstream indoor wireless technologies as WiFi, Zigbee, and Bluetooth. For example, Apple's smart wearables use WiFi/Bluetooth for data exchange; Google Home uses WiFi for media content download and ambient sensor control, including NEST thermometers, smoke alarms, and cameras. As there are numerous and diverse IoT sensors to be deployed, a critical challenge that these communication technologies face is power consumption, particularly given that many of the devices are battery powered, which has long been a concern in sensor networks.

A sea-change comes with the *backscatter communication* [1], which uses RF reflection rather than a proactive transceiver,

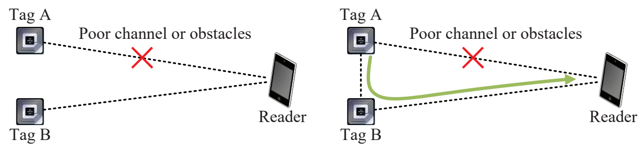

(a) Single-hop backscatter (b) Multi-hop backscatter

Figure 2: A comparison of single-hop and multi-hop backscatters: multi-hop provides path diversity and robustness for tag data transmission.

thus considerably reducing the power consumption. In particular, Radio Frequency IDentification (RFID) tags, as a zero-power solution with extremely low cost, have largely expanded their use in the retail industry. In a backscatter system, a tag with built-in programmable hardware and modulation circuitry works by changing its antennas' impedance, deciding whether to reflect an excitation signal or not. The excitation signal is usually generated by an external reader, which also decodes the backscattered signal to obtain the information from the tag. Besides using dedicated readers, recent studies have demonstrated that such ambient signals as TV, FM, cellular, visible light, LoRa, and even WiFi, can be used for excitation as well [2, 5, 6, 9, 14–16, 28, 29, 32–34].

Backscatter communication offers a cost- and energy-efficient means for IoT sensor data exchange. Pioneer works on enabling backscatter for cross-protocol communications, smart devices, and on-body or implanted sensors, such as Inter-Technology Backscatter [5], FS-Backscatter [6], Hitch-Hike [7], BackFi [3] and FreeRider [30], have tackled many compatibility and deployment issues therein. Yet they all operate in a single-hop mode, i.e., the sensing tags do not relay for each other. The restricted connectivity however can severely limit the robustness and scalability of backscatter communication, and more importantly, falls short of the IoT vision of ubiquitous interconnection.

Back to traditional network design, such fundamental challenges as robustness, throughput, and scalability are often tackled from building end-to-end path diversity. Typical examples include datapath adaptation in multi-hop sensor networks [38], and multipath transmission in datacenters and heterogeneous wireless networks [39–41]. We naturally ask: can backscatter communication benefit from path diversity? Figure 2 compares single-hop and multi-hop backscatters. If the direct path from Tag A to Reader fails, single-hop backscatter cannot receive data from Tag A. In contrast, multi-hop backscatter can use Tag B's relay as a backup path in the same situation. We observe in our experiments that tag relay can successfully tackle unreliable channels, especially when densely deployed tags encounter physical obstacles, like moving human, walls, and indoor facilities. Motivated by this observation, we explore multi-hop backscatter,

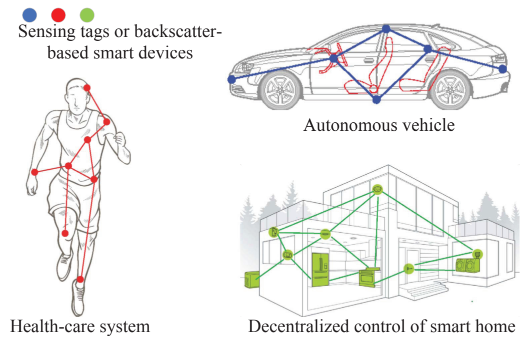

Figure 3: Potential IoT applications of multi-hop backscatter.

which not only provides path diversity and robustness, but also promisingly leads to multipath routing and transport in backscatter networks. Potential applications span from robotic monitoring, indoor/outdoor 3D mapping, to retail stores with RFID infrastructures, as well as many other multi-hop IoT scenarios, e.g., health-care with on-body sensing tags for data collection, autonomous vehicles that require robust sensor data transmission, and decentralized smart home with control from anywhere, as shown in Figure 3.

In this paper, we present X-Tandem, a multi-hop backscatter communication system working with commodity WiFi. X-Tandem not only provides the compatibility with off-the-shelf WiFi devices, but also enables packet relays among multiple tags, which modulate their sensing data into a single backscattered packet. This backscattered packet, though carrying diverse data fields for multiple tags, is constructed as a strictly legit WiFi packet. Figure 1 illustrates the key operations: Assume there is an ongoing WiFi signal, the first tag uses this original WiFi signal as an excitation and modulates the sensing data onto it; The second tag, upon receiving the backscattered signal from the first tag, relays the first tag's data and keeps embedding its data onto the same backscattered signal. The backscatter receiver (a commodity WiFi device) then decodes all the tags' data by code-translating the backscattered WiFi data from a clean receive channel. During this multi-hop process, the normal WiFi communication is entirely unaffected thanks to a frequency shift design.

Designing such a multi-hop backscatter system faces the following challenges:

- The multi-hop mode in Figure 1 follows a Tag1-Tag2-Tag3-...-Tag$n$-AP (reader) route, involving a series of intermediate backscattered signals (e.g., the first-hop signal from Tag1 to Tag2) and the associated extra decoding operations as compared to the basic single-hop (tag-to-reader) mode. Since these signals spread within WiFi bands, our multi-hop backscatter system has to deal with not only the interference between the excitation and backscattered signals, but also the interference among multiple hops.

- Multi-hop tag modulation in a packet entails a series of operations for tag hardware configuration, such as assigning a route and synchronizing multiple tags information to specific data fields. These operations demand an efficient control mechanism, preferably with no extra hardware for decoding, as compared to previous single-hop WiFi backscatter solutions.
- The excitation signal can be reflected multiple times among the tags, during which out-of-order reflection can occur. In particular, when the tags are close to each other, the impact of the out-of-order backscattered packets will be non-negligible during decoding.

Our X-Tandem is a framework of multi-hop backscatter that enables tag relay using analog forwarding with decoding-free tags (i.e., a tag does not decode the incoming information from other tags). Our tag design is different from the decoding-enabled tag in Ambient Backscatter [16]. In particular, an Ambient Backscatter tag digitally decodes the backscattered signals, while our tag simply forwards the backscattered signals from previous hops in an analog way without decoding. Despite the signal attenuation issue in analog forwarding, our solution (i) has much less hardware complexity for the tag because decoding backscattered signals is not required; (ii) is able to perform tag relay and tag modulation simultaneously; and (iii) uses only commodity radios to decode multiple tags information. The main technical contributions of our work are summarized as follows

- To relay among multiple tags, we introduce a Multiple Frequency Shifts (MFS) scheme, which enables an original WiFi packet to be backscattered for more than once. Within each hop, we keep the backscattered frequency far away from the incoming frequency, avoiding affecting the data from previous hops.
- To coordinate the multi-hop transmission, we design a smart data field allocation mechanism, which (i) uses control signals to specify the order of tags for backscattering, and (ii) allocates a packet's data fields for different tags.
- We also design a packet verification scheme that eliminates out-of-order backscattered packets using RSSI measurements while keeping in-order backscattered packets intact.

To verify our design, we have built a hardware prototype of X-Tandem, which works with 802.11b/g/n WiFi signals. Each tag integrates an FPGA, frontend analog circuits and other modules for the extended functions, e.g., drive circuits of connected sensors. The current prototype demonstrates a two-hop implementation (i.e., tag 1 to tag 2 and tag 2 to an AP), in which the tag-to-tag distance is within a limited range due to multi-hop path attenuation. Our experiments show that X-Tandem significantly improves the backscatter communication quality and range when encountering obstacles. It achieves a two-hop throughput up to 200 bps with inter-tag distances up to 0.4 m and communication ranges up to 8 m. To improve the communication range and network size, we also discuss the potential extensions, e.g., using LoRa for long range backscatter communication. Finally, an environment monitoring system, using temperature/humidity sensors, X-Tandem tags and commodity WiFi devices, further demonstrates the applicability of our design.

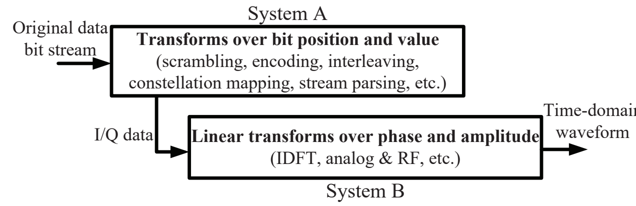

Figure 4: WiFi transmitter.

2 WIFI PHY: RELATED BACKGROUND

We use 802.11b/g/n WiFi as the excitation signal for X-Tandem. We first briefly introduce the system architecture of WiFi transmitter [44–47]. This is a necessary preliminary to Subsection 3.2, where we will illustrate why a multi-hop backscatter packet in our X-Tandem design is still a legit WiFi packet. As illustrated in Figure 4, a WiFi transmitter includes two main systems: System A first maps the original data bit stream to the I/Q data with amplitude and phase in the constellation; The I/Q data is then input into System B to generate RF signals that can multiplex frequency or space at the carrier's central frequency.

System A includes scrambling, barker coding and constellation mapping in 802.11b, and scrambling, convolutional encoding, interleaving and constellation mapping in 802.11g. In both of them, System A is linear over the original data bit's position and value. Advanced WiFi standards (802.11n and beyond) have introduced spatial multiplexing and added a spatial stream parser in System A, which then becomes non-linear since the stream parser assigns consecutive data bits to different spatial streams in a round robin manner. In Subsection 3.2, we will see that, an X-Tandem tag has up to four types of phase modulation if System A is linear, but only two types if System A is non-linear.

System B includes such transforms as Inverse Discrete Fourier Transform (IDFT) for OFDM, time-domain windowing, and baseband to carrier frequency. It is linear over the I/Q data vector space, which means a phase change on the time-domain waveform will be converted to a phase change on the I/Q constellation points.

3 X-TANDEM DESIGN

The key challenge toward implementing multi-hop WiFi backscatter lies in the mutual interference between excitation and backscattered signals, multi-hop tag modulation in

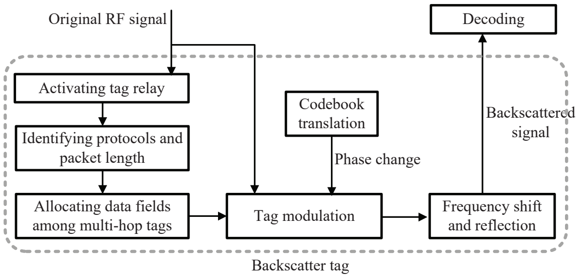

Figure 5: Overview of system design.

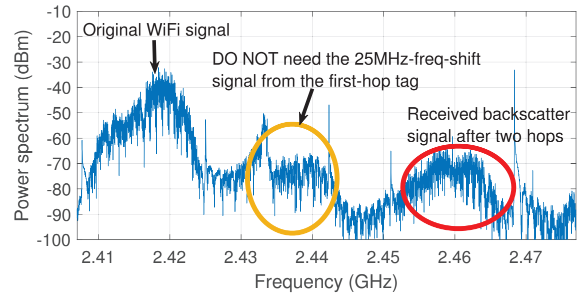

Figure 6: Two-hop backscatter signal's power spectrum over the 2.4GHz frequency band. Each tag uses 25MHz frequency shift, thus backscattering the original WiFi signal from 2.417GHz (Channel 2) to 2.467GHz (Channel 12). Only the last-hop backscattered signal is used for decoding.

a single packet, and out-of-order backscattered packets. The use of commodity WiFi further imposes strict compatibility requirement. Our X-Tandem addresses it through a set of cascaded smart operations, including multiple frequency shifts, adaptive field allocation and RSSI-based packet verification.

This section demonstrates the design details of X-Tandem, with a modular overview of the system showing in Figure 5. A WiFi sender first generates the control signals, from which the tag's frontend analog circuits can capture the activating commands and the pre-defined packet duration patterns. Such information will be used in the following FPGA modules to identify the type of network protocols. These control signals decide how to assign a route and allocate data fields for multiple tags. The original excitation signal from the sender is then fed into the tag modulation module. The codebook translation ensures that the tag-modulated data can still be demodulated from the constellation of WiFi. The frequency shift enables the last-hop backscattered signal to be received from a clean and less-occupied channel away from previous hops frequency band. Finally, a WiFi receiver decodes multiple tags' multiple bits data from each last-hop backscattered packet.

3.1 Tag Relay by Multiple Frequency Shifts

X-Tandem uses multiple times frequency shift (MFS) to do relays among tags. With this MFS scheme, a multi-hop backscattered signal can be received at the frequency band far away from the excitation signal, and it is not affected by previous hops' signal, either. Without loss of generality, we illustrate this with the two-hop case. The first hop tag performs backscattering by multiplying the original excitation RF signal with a square wave signal, and the second hop tag relays the first hop tag's backscattered signal by multiplying it with another square wave signal. Let $M_{tag}^{(1)}(t) = \frac{4}{\pi}\sum_{n=1}^{\infty}\frac{\sin((2n-1)\omega_1 t)}{2n-1}$, $M_{tag}^{(2)}(t) = \frac{4}{\pi}\sum_{m=1}^{\infty}\frac{\sin((2m-1)\omega_2 t)}{2m-1}$ be the square wave signals, used by the first hop tag and the second hop tag, respectively. Let f_c be the center frequency of the excitation signal, and f_1 and f_2 be the square wave frequencies of the first hop tag and the second hop tag, respectively. Let $\omega_c = 2\pi f_c$, $\omega_1 = 2\pi f_1$, $\omega_2 = 2\pi f_2$, $\alpha_{base}(t)$ be the baseband waveform of the excitation signal, and $\beta(t)$ be the multi-hop backscattered signal. Two frequency shifts are as follows

$$\begin{aligned}\beta(t) &= \alpha_{base}(t)\sin(\omega_c t)M_{tag}^{(1)}(t)M_{tag}^{(2)}(t)\\ &= \frac{4}{\pi^2}\alpha_{base}(t)\Bigg(\sum_{m=1}^{\infty}\sum_{n=1}^{\infty}\frac{1}{(2n-1)(2m-1)}\\ &\quad\cdot\Big\{\sin((\omega_c-(2n-1)\omega_1+(2m-1)\omega_2)t)\\ &\quad-\sin((\omega_c-(2n-1)\omega_1-(2m-1)\omega_2)t)\Big\}\\ &\quad-\sum_{m=1}^{\infty}\sum_{n=1}^{\infty}\frac{1}{(2n-1)(2m-1)}\\ &\quad\cdot\Big\{\sin((\omega_c+(2n-1)\omega_1+(2m-1)\omega_2)t)\\ &\quad-\sin((\omega_c+(2n-1)\omega_1-(2m-1)\omega_2)t)\Big\}\Bigg)\end{aligned} \tag{1}$$

We analyze the backscattered signal by considering the fundamental component of the square waves, i.e. $n = 1$ and $m = 1$, which follows:

$$\begin{aligned}\beta(t) = \frac{4}{\pi^2}\alpha_{base}(t)\Big(&\sin((\omega_c-\omega_1+\omega_2)t)-\sin((\omega_c-\omega_1\\ &-\omega_2)t)-\sin((\omega_c+\omega_1+\omega_2)t)+\sin((\omega_c+\omega_1-\omega_2)t)\Big)\end{aligned} \tag{2}$$

Let $F_{base}(\omega)$ be the Fourier transform of $\alpha_{base}(t)$, and F_ω be the Fourier transform of $\beta(t)$. When the two tags have the same implementation, let $\omega_1 = \omega_2 = \omega_t$, and we have

$$\begin{aligned}F(\omega) = \frac{2j}{\pi^2}\Big(&2F_{base}(\omega+\omega_c)-2F_{base}(\omega-\omega_c)\\ &-F_{base}(\omega+\omega_c-2\omega_t)+F_{base}(\omega-\omega_c+2\omega_t)\\ &-F_{base}(\omega+\omega_c+2\omega_t)+F_{base}(\omega-\omega_c-2\omega_t)\Big)\end{aligned} \tag{3}$$

The backscattered signal is received at the frequency spectrum $|F(\omega-\omega_c-2\omega_t)|$. Figure 6 shows the spectrum we capture from the original and backscattered signals. We can

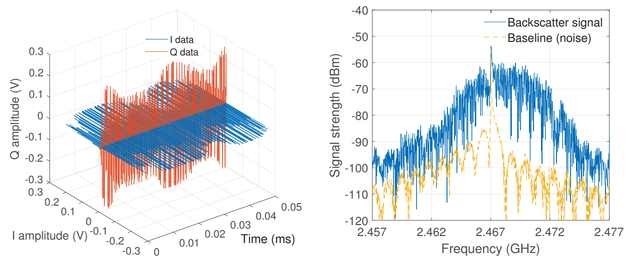

(a) Backscattered I/Q signal in time domain (b) Backscattered signal at central frequency 2.467GHz

Figure 7: Two-hop backscattered WiFi signal captured at the 2.467GHz: 50MHz frequency shift from original WiFi signal at 2.417GHz.

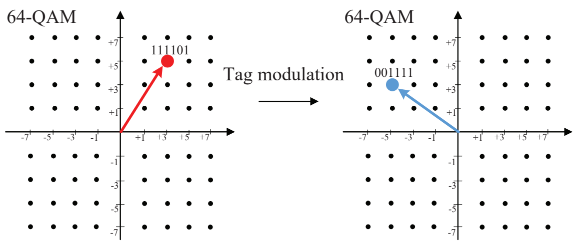

Figure 8: The backscattered data still falls in the constellation of 64-QAM when tag modulation uses 90° **phase change .**

see that the backscattered signal is 50MHz away from the original signal. The first-hop (25MHz frequency shift) signal in the spectrum does not interfere the backscattered signal, and it is also useless in decoding the tag data. This is further illustrated in Figure 7, which gives the captured signal in both the time domain and the frequency domain.

3.2 Multi-hop Tag Modulation in a Packet

In addition to tag relay, X-Tandem also enables multi-hop tags to embed their data simultaneously in a single WiFi packet. We will illustrate how to modulate the tag data in a packet and how to do this for multi-hop tags.

Tag modulation in X-Tandem adopts the codeword translation method proposed in [7], which has been implemented and evaluated in the backscatter systems using WiFi 802.11b [7], 802.11g/n OFDM, Bluetooth, Zigbee [30], and 802.11n MIMO-OFDM double streams [37]. This method can be illustrated with the example in Figure 8. The tag modulation makes phase change on the original signal's data fields. The backscattered data after tag modulation still falls in the constellation of the original data. For commodity radio protocols such as WiFi, this means that the backscattered signal can be decoded with a commodity radio device.

To illustrate why such phase change keeps data in the same constellation, we use the WiFi transmitters in Figure 4 as an example. For 802.11b/g and 802.11n single-stream, System A and System B in Figure 4 are linear transforms of phase change. Let H be a transform that includes all the operations, e.g., scrambling, encoding, and IDFT. Let X be the original data and $Y(t)$ be the time-domain waveform carrying X. We have $Y(t) = H(X)$. Let θ be a tag's phase change operation on $Y(t)$. The tag modulation is as follows:

$$\theta \cdot Y(t) = \theta \cdot H(X) = H(\theta \cdot X). \tag{4}$$

As the receiver has inverse operations H^{-1}, the backscattered data is θX. If we choose the phase change properly, θX will fall in the same constellation. For 802.11n multi-stream case, the transmitter however introduces a stream parser that assigns data to multiple spatial streams in a round-robin manner and becomes a non-linear transform of phase change. Yet phase change $0^\circ/180^\circ$ can still be used to embed one bit tag data on a packet. The choice of phase change for different protocols is summarized as a tag codebook in Table 1.

Table 1: Tag codebook for different protocols.

Protocol	Barker or subcarrier modulation	Phase change	Tag data
802.11b	DBPSK	0°	0
		180°	1
	DQPSK, CCK	0°	00
		90°	01
		180°	10
		270°	11
802.11g, 802.11n single stream	BPSK	0°	0
		180°	1
	QPSK, 16QAM, 64QAM	0°	00
		90°	01
		180°	10
		270°	11
802.11n multi-stream	2/4/16/64QAM	0°	0
		180°	1

Based on the modulation method above, there are two available ways to modulate multi-hop tags information into one packet. The first is to change the phase of the same packet data fields multiple times, corresponding to multiple tags modulation. Another is to separate the data fields into pieces and allocate them to different tags. While the former has the potential to embed more data bits for a tag, it needs every hop backscattered signal for decoding, and tags depend on each other in modulation. In contrast, the latter only needs the last hop backscattered signal, and tags are mutually independent. As such, we choose the latter and propose the following data fields allocation mechanism.

3.3 Packet Data fields Allocation among Tags

3.3.1 How to separate the data fields? A wireless packet is a time-domain waveform that includes both the payload data

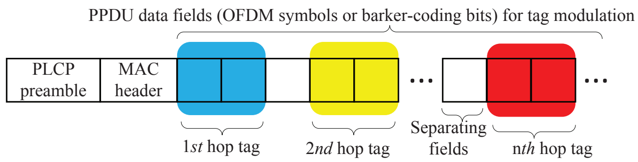

Figure 9: An original packet's data field allocation for multiple backscatter tags.

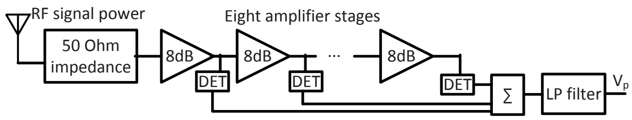

Figure 10: RF signal power detector.

and the header information for addressing, synchronization, etc. Different packet formats correspond to different protocols and physical layer specifications. Taking an 802.11n WiFi packet as an example, it corresponds to a Physical Layer Convergence Procedure (PLCP) frame structure that includes a PLCP preamble field, a MAC header field, and a PLCP Protocol Data Unit (PPDU) data fields. The PPDU data fields include a variable number of OFDM symbols, each of which contains the same number of bits of the coded data and has a fixed symbol duration. We use the PPDU data fields to carry multiple tags' information, as shown in Figure 9. Each part is assigned to one tag, following the order of hops. Let L_{packet}, $L_{preamble}$, L_{header}, and L_{data} be the packet length, PLCP preamble length, MAC header length, and PPDU data fields' length, respectively. The length here is calculated by the duration of waveforms, which, for the data fields, is given by:

$$L_{data} = L_{packet} - L_{preamble} - L_{header}. \tag{5}$$

Let L_s be the total length of the separating fields. Suppose that the ith ($i \in \{1, 2, ..., m\}$) hop tag uses n_i OFDM symbols to carry one bit tag data. Let N_i^{tag} be the number of bits of the ith hop tag data embedded in a packet, and it is calculated as follows:

$$N_i^{tag} = \left\lfloor \frac{L_{data} - L_s}{m \cdot n_i \cdot T_{sym}} \right\rfloor \tag{6}$$

where T_{sym} is the symbol duration.

3.3.2 How to obtain packet length? In X-Tandem, the tag's frontend analog circuits use an RF power detector to convert the incoming RF power signal to an equivalent DC voltage. Figure 10 is an example of the detector design. A 50 Ohm impedance matching network is used to absorb the 2.4GHz frequency band signal. The following component is a multistage power amplifier that consists of multiple 8dB amplifiers and diode detectors. The multistage amplifier outputs are summed up and then fed into a low pass filter, where the output voltage V_p is proportional to the detected signal strength

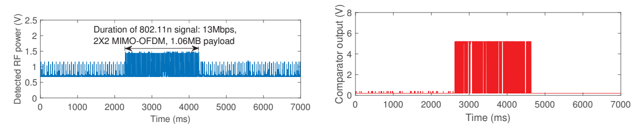

(a) Detector output (b) Comparator output

Figure 11: RF power detector outputs and voltage comparator outputs when transmitting 1.06M Bytes payload data. (a) The detector converts the RF power to an equivalent DC voltage. (b) The comparator uses a voltage threshold to filter noise and obtains signal duration.

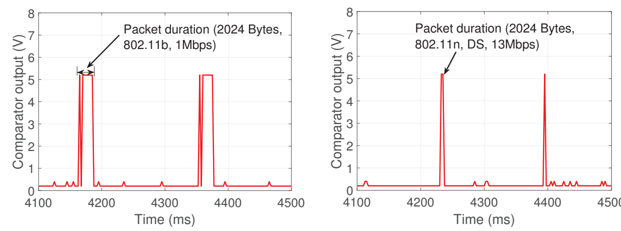

(a) 802.11b (b) 802.11n

Figure 12: Different protocols' packet durations obtained from the voltage comparator.

P_{RF}. V_p can be formulated as follows:

$$V_p = K \cdot P_{RF} \tag{7}$$

where the scale factor K is a constant in the operating range between the intercept and the saturation points.

Figure 11(a) shows the trace captured from the RF power detector during the transmission of 1.06M byte payload data using 802.11n WiFi. We can see that the detector can capture the key features of the RF signal, including the start time, the end time, and the duration of the signal. Since different protocols exhibit different durations when transmitting the same amount of data, the signal duration can be used to identify protocols.

To eliminate the noise voltage in Figure 11(a), another necessary component is a voltage comparator, which converts the detector's output voltage to a binary-level voltage. Figure 11(b) shows the comparator output after filtering the noise in Figure 11(a).

The comparator generates a positive/negative edge for the start/end time of the RF signal, which can also be used to detect the duration of a packet. Figure 12 shows the comparator's outputs for individual packets, each transmitting 2024 Bytes payload data with different protocols. When such signal is fed into the FPGA, the FPGA can use a counter with clock frequency to calculate the packet duration.

3.3.3 How to generate control signals? X-Tandem needs to specify whether to perform tag relay or not and which tag to

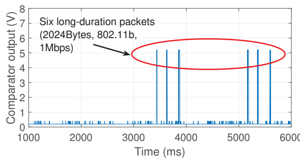

(a) Tag relay on

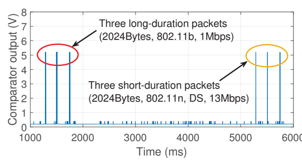

(b) First hop: tag '01'

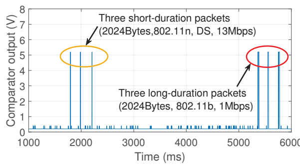

(c) First hop: tag '10'

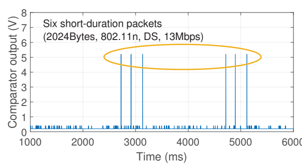

(d) Tag relay off

Figure 13: Four types of control signals received by a tag: (a) tag relay is on; (b) the tag with ID '01' is the first hop; (c) the tag with ID '10' is the first hop; (d) tag relay is off.

be the first hop (according to Subsection 3.3.1, the first hop and the second hop have different tag modulation fields in a packet). To achieve this, we design four control commands and use the excitation source to generate the corresponding control signals for the tags. In Figure 13, a long packet is of 2024 Bytes payload using 802.11b 1Mbps, and a short packet is of 2024 Bytes payload using 802.11n Double Streams (DS) 13Mbps. Given tag IDs '01' and '10', the four control signal patterns are: (i) six long packets indicating that tag relay is switched on; (ii) three long packets followed by three short packets indicating that tag '01' is the first hop; (iii) three short packets followed by three long packets indicating that tag '10' is the first hop; (iv) six short packets indicating that tag relay is switched off. An X-Tandem tag uses a customized module of the FPGA circuits to detect the above control signals, which will be further explained in Section 4.

3.4 Tag Data Decoding

Multi-hop tag data decoding takes three steps. In the first step, we design a packet filter to cancel the out-of-order backscattered packets from all the received backscattered packets. Typical out-of-order backscattering scenarios are illustrated in Figure 14(a). As discussed in Subsection 3.3.3, the tags will be given the hop order after receiving the control signals. There are however packets backscattered initially by the second hop tag near the RX and then backscattered by the first hop tag near the TX. To filter these packets, we propose a packet verification scheme that captures the packet RSSI information and utilizes the RSSI difference between the in-order and the out-of-order packets. Figure 14(b) is a typical example showing that there is significant RSSI difference between two types of packets. We can set an RSSI threshold

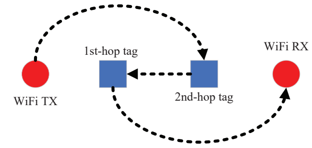

(a) Out-of-order tags

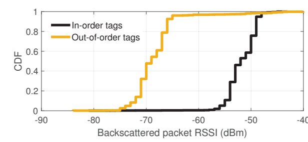

(b) Packet RSSI

Figure 14: Backscattered packet's RSSI of in-order tags and out-of-order tags. The RSSI information can be used to filter the out-of-order tags' backscatter signal.

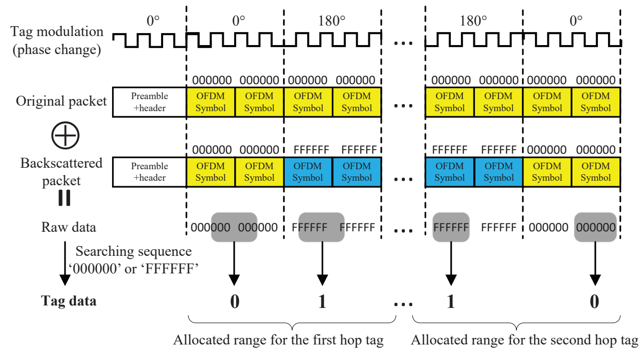

Figure 15: Decoding both tags data from a backscattered packet.

to filter more than 95% of the packets from out-of-order tags. This step is necessary for static tag deployment with fixed routing (hop order), e.g., monitoring tags on bridges or buildings, and implanted sensors.

The next two steps are illustrated in Figure 15. In the second step, we use the XOR operation decoder proposed by [7]. For 802.11g/n, we carry out the third step to search the tag bits from the OFDM symbols. The third step uses the algorithm of all-zero or all-one sequence searching proposed by [37] in the allocated fields for each tag.

3.5 Mode Switch and Fault Tolerance

X-Tandem can work in either the relay mode or the direct communication mode, and has the flexibility to switch when necessary. As we have introduced in Subsection 3.3, X-Tandem uses control signals to switch on/off the function of tag relay. As shown in Figure 16(a), when direct communication between a tag and the reader fails due to channel failure, X-Tandem tag relay can work as a backup path. Further, as shown in Figure 16(b), the tag relay can mitigate the impact of physical obstacles, like moving human bodies, walls, furniture and floors. In Section 5, we will evaluate how X-Tandem can improve the communication quality in such scenarios. Furthermore, while enabling tag relay, the tags should keep mutual independence. In X-Tandem, each tag modulates information independently, and hence it is not affected by other tags' abnormal operations, e.g., a damaged

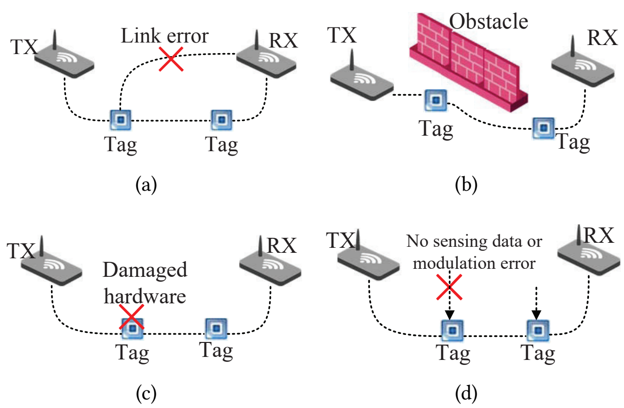

Figure 16: Enhancing backscatter communication quality and robustness by multi-hop tags: the tags are mutually independent but can relay for each other.

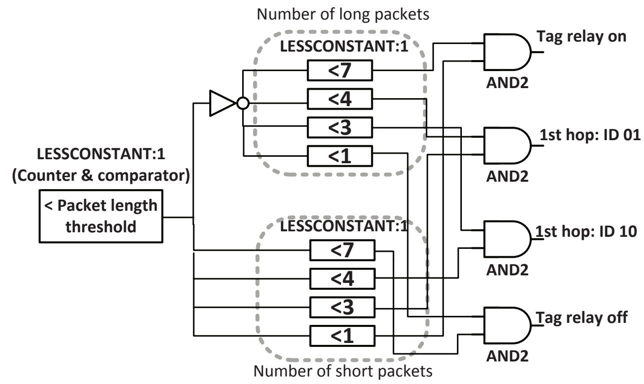

Figure 17: FPGA circuits of detecting control signals, assigning a route, and switching modes.

tag in Figure 16(c) and bit errors of a tag in Figure 16(d). When the sensing tags are densely deployed in challenging scenarios (e.g., indoor facility obstacles, human obstacles, or harsh-environment applications), these fault tolerant designs can better accommodate unreliable channels and improve the transmission robustness.

4 IMPLEMENTATION

4.1 Frontend Analog Circuits

X-Tandem tag's frontend analog circuits include an RF signal power detector and a voltage comparator. We implement these circuits using off-the-shelf ICs and periphery components (e.g., matching impedance, low-pass filters, and threshold voltage configuration). The RF power detector uses AD8313, a multistage demodulating logarithmic amplifier that can convert an RF signal to an equivalent DC voltage in high accuracy (1.0 dB over 65 dB range) and short signal response time (40ns) with low power supply (2.7V). The voltage comparator uses TLV3501, which works with high switching speed (4.5ns propagation delay, 1.5ns rise time and 1.5ns fall time) and low power supply (2.7V). We use a sliding rheostat on the tag circuit board to set the comparator's threshold, which for the first hop tag is 1.25V and, for the second hop tag, decreases to 1.1V given the distance between the two tags increases.

4.2 FPGA Modules of Control Signal Detection and Data Fields Allocation

We use a WiFi TX to first generate the control signals for the two tags with IDs '01' and '10', respectively. After receiving the control signals from the frontend analog circuits, each tag uses an FPGA digital circuit module to detect these specific signal patterns, so as to follow the assigned route and calculate the modulation range of data fields. In our implementation, the control signals are set as follows: (i) 6 long packets (11b 1Mbps 2024B payload) to switch on tag relay; (ii) 6 short packets (11n DS 13Mbps 2024B payload) to switch off tag relay; (iii) 3 long packets first, followed by 3 short packets to indicate tag '01' as the first hop tag; and (iv) 3 short packets first, followed by 3 long packets to indicate tag '10' as the first hop tag. We implement the module in a XILINX Spartan XC3S500E-4PQ208 FPGA. Figure 17 shows the main components of the control signal detecting module. The LESSCONSTANT:1 blocks are used in the RTL schematic of XILINX's synthesize tool XST, and each of them incorporates a counter and a digital value comparator. The first LESSCONSTANT:1 block recognizes a long or short packet according to its duration, and then the following LESSCONSTANT:1 blocks calculate the number of long or short packets, which creates the mentioned control signal patterns.

After the control signals, the two tags will receive the predefined packets with fixed bits of payload data. These packets are used to identify protocols and calculate the modulation range allocated in the packet data fields. Figure 18 shows the three main processing parts in order. The first part of the circuits is an example of identifying the used protocol from two candidates. Each LESSCONSTANT:1 block decides whether a packet duration falls below its decision threshold (corresponding to a specific protocol). The FDPE flip-flop outputs '0' if packet duration is less than the threshold, and outputs '1' otherwise. Then the counters in the second part are used to calculate the data fields length. Finally, the third part of the circuits executes the one bit right-shift operation to halve the length of the second part output. The third part output is used for the following operations in data fields allocation, e.g., minus the separating symbols and localizing the start position. For ambient WiFi excitations with random packet length, the control signals can still be generated in the same way, but an extra WiFi device is needed to analyze ambient packets (protocols and lengths) and notify the tags.

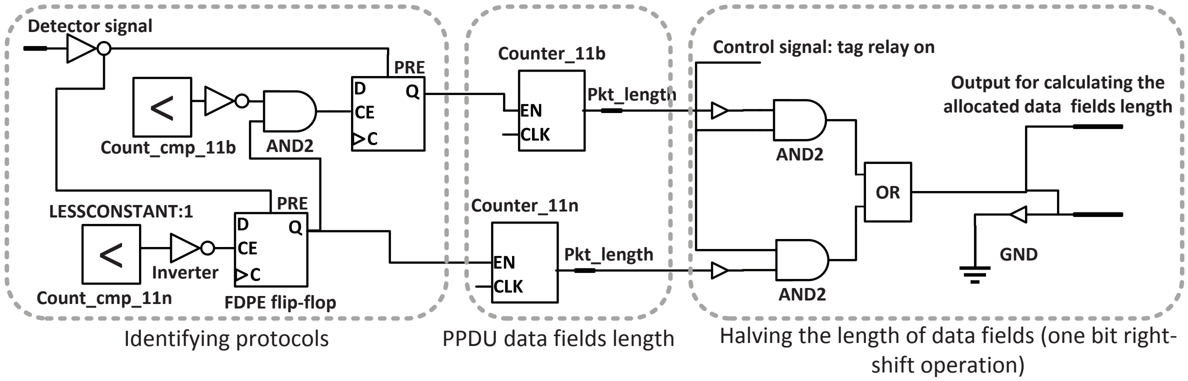

Figure 18: FPGA digital circuits of calculating the length of packet data fields allocated to a tag.

4.3 FPGA Modules for Tag Modulation

Figure 19 shows the main components of the tag modulation circuits. The tag's frontend circuitry outputs a positive edge to trigger tag modulation when it detects WiFi signal power. Then the data fields allocation module outputs the start position (from the end of the PLCP preamble for the first hop tag, or from the end of separating fields for the second hop tag) and the length of the allocated data fields. When synchronizing to the start position, the tag will modulate the OFDM symbols one by one with phase change following the codebook in Table 1. Tag modulation's frequency shift uses a 25MHz clock if tag relay is on, and 50MHz otherwise. The varying phase of 25MHz square waveform is achieved using a XILINX FPGA's Digital Clock Manager (DCM) IP core. The 4-input multiplexer is used to select from the four phases 0°, 90°, 180° and 270°, and its output controls the following RF switch ADG902. The tag does not modulate data during the possible idle slots of ambient WiFi transmissions.

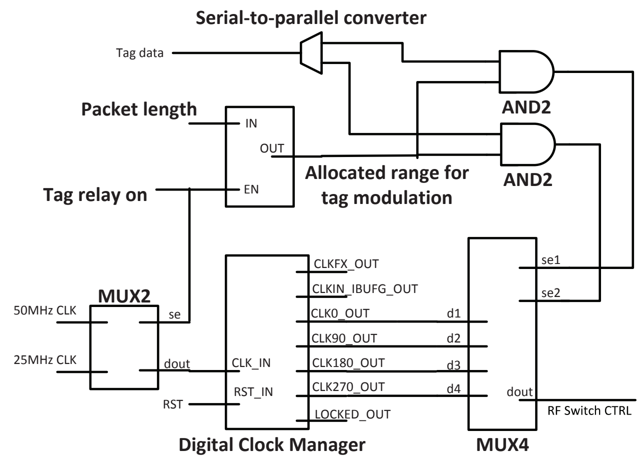

Figure 19: FPGA circuit of tag modulation.

4.4 Synchronization

The synchronization of tag modulation is from the following aspects. First, the WiFi TX sends a specific pattern of consecutive packets to synchronize with the tags. In our implementation, the pattern is of eight packets that represent 'long, short, long, short, long, short, long, short', where the long packet uses 2024B 1Mbps 802.11b and the short packet uses 2024B 13Mbps DS 802.11n. After detecting this pattern, the tag begins to modulate from the next positive edge signal. Second, tag modulation needs to skip (just do frequency shift and do NOT change the phase) the PLCP preamble. We use a counter with the FPGA's internal clock input to calculate the number of clock positive edges equivalent to the preamble duration. For 802.11b signals, the PLCP preamble is 192μs, the MAC header is 192μs, and each data bit is 1μs. For 802.11g signals, the PLCP preamble is 20μs, the MAC header is 16μs, and each OFDM symbol is 4μs. For 802.11n signals, the PLCP preamble is 32μs, the MAC header is 16μs, and each OFDM symbol is 4μs. Third, the WiFi RX listens to the channel of backscattered signals, and it only receives the backscattered packets that have the WiFi TX's address as its source address in the MAC header. The WiFi TX/RX devices are Dell OptiPlex 7010 equipped with Qualcomm Atheros AR938x wireless network adapter. The WiFi traffic generator is the software tool CommView for WiFi[1] for 802.11 a/b/g/n/ac wireless network packets generation, reception and analysis. In our implementation, CommView for WiFi at the RX side works in the single-channel scanning mode, and it scans channel 12 (2.467GHz) since we generate the excitation signal from channel 2 and the two tags both have 25MHz frequency shift.

4.5 Extended Function

The X-Tandem tag prototype is shown in Figure 20(a). The extended function includes the sensing capability and self-sustainable power supply. The free input/output/inout ports of the XC3S500E FPGA are connected to the on-board pins,

[1]http://www.tamos.com/products/commwifi/

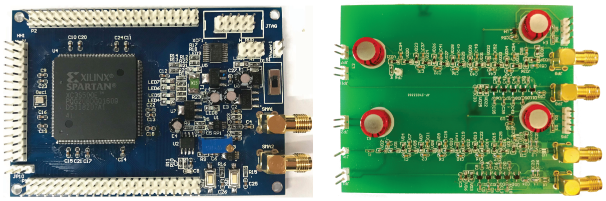

(a) Tag prototype (b) WiFi energy harvester

Figure 20: X-Tandem tag prototype and an energy harvesting circuit board.

which can be connected to other periphery circuits or components, e.g., accelerometers, humidity and temperature sensors. When using these external sensing devices, we also need the FPGA drive modules to receive the sensing data and convert them into tag bit stream. We also build a WiFi energy harvesting board as shown in Figure 20(b)[2]. The main components include a multi-layer chip band pass filter BF2012-L2R4DART/LF that provides the matching network with antennas, a six-stage SMS7621 Schottky rectifier circuit that works as an RF-DC converter, and LX 0.1F Maxcap double layer capacitors that store the energy. When placing this harvester near ambient WiFi transmitters (e.g., a WiFi AP), charging it for 4.1 volts usually takes several hours, which depends on ongoing traffic load. While the harvester works within the tag's operating voltage range (2.7~5V), it has a limited charging speed and currently only works as a backup power supply. The current implementation of X-Tandem tags still needs an external power supply to achieve stable performance and all the experiments in section 5 use a 5V power supply.

4.6 Power Analysis

We use the tool XPower in Xilinx Integrated Synthesis Environment version 14.7 to analyze the power consumption of FPGA. The X-Tandem tag prototype in Figure 20(a) uses the FPGA to implement the phase modulation circuit, the control signal detection circuit, the data field allocation circuit, and the drive circuits for external sensors. The total power consumption is 14.2 mW, which is mainly consumed by the DCM IP core for phase modulation. Since the DCM is energy-hungry, our further work may replace it with the power-efficient frequency shifting designs, such as the ring oscillator [6] and the low-power phase-lock loop [5]. The tag prototype can also adopt analog modulation circuits and low-power FPGAs[3]. The power consumption can be further

[2]Refer to [8] for the basic principles and some practical design examples of RF energy harvesting technology.

[3]https://www.xilinx.com/products/technology/power.html
http://www.actel.com/FPGA/handheld/?p=sn

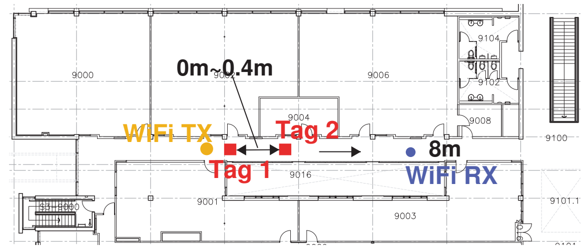

Figure 21: Experiment scenarios of evaluating X-Tandem performance change with distance.

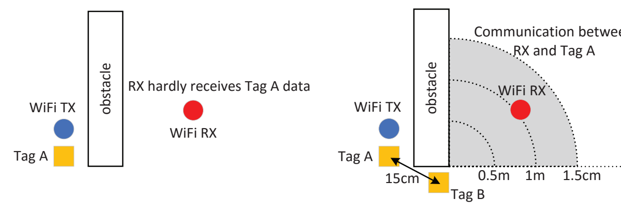

(a) No tag relay (b) Tag relay

Figure 22: Experiment scenarios of using tag relay to improve communication quality.

reduced to tens to hundreds of microwatts using IC design [5–7, 28, 30, 33, 36].

5 EVALUATION

In this section, we evaluate the performance of X-Tandem in different experiment scenarios. We examine how the two-hop backscattered signal strength, communication throughput and tag data bit error rate change with both tag-to-RX distances and tag-to-tag distances. We also study how X-Tandem utilizes tag relay to enhance the performance when encountering obstacles between a single-hop tag and a backscattered signal receiver.

5.1 Experiment Setup

Figure 21 shows the experiment scenario of communication ranges in a 33m×15m indoor area. The experiment configurations are illustrated as follows. X-Tandem tags and WiFi transmitter and receiver devices are all placed in the corridor as shown in the floor plan. In the first experiment, the WiFi transmitter and the two tags have fixed positions, and the WiFi receiver moves along a straight line to increase the distance away from the tags. In the second experiment, we do not change the positions of the transmitter, the receiver and the first-hop tag, but move the second-hop tag along the corridor to increase the distance from the first-hop tag. Figure 22 shows the obstacle experiment scenario that compares the single-hop and two-hop backscatter communications. The Received Signal Strength Indicator (RSSI), Bit Error Rate (BER) and throughput are measured in all the experiments.

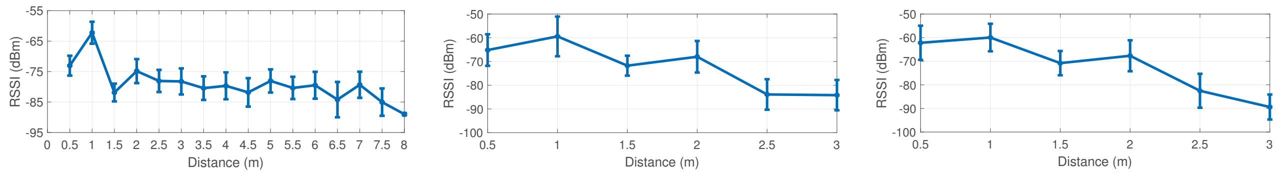

(a) 802.11b 1Mbps (b) 802.11g 6Mbps (c) 802.11n SS 6.5Mbps

Figure 23: Received backscatter signal strength change with distance between tags and WiFi RX.

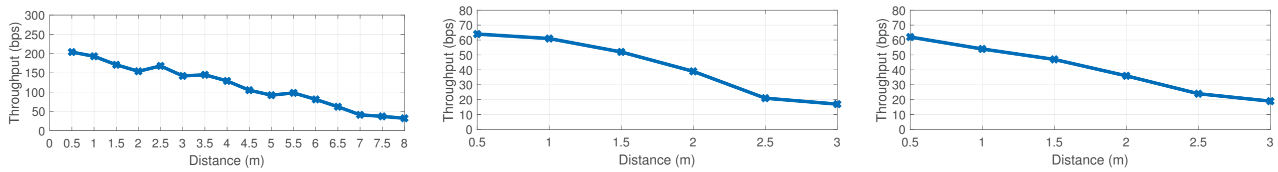

(a) 802.11b 1Mbps (b) 802.11g 6Mbps (c) 802.11n SS 6.5Mbps

Figure 24: Backscatter throughput change with the distance between tags and WiFi RX.

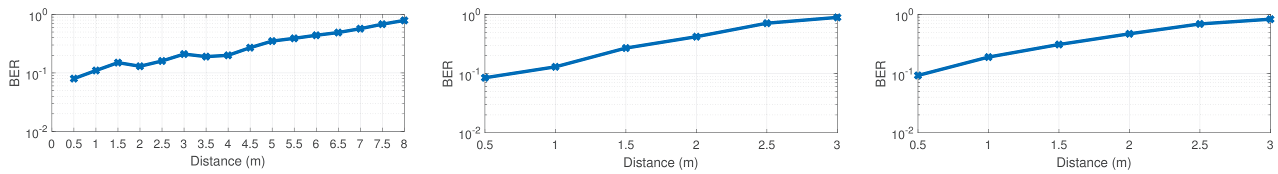

(a) 802.11b 1Mbps (b) 802.11g 6Mbps (c) 802.11n SS 6.5Mbps

Figure 25: Tag bit error rate change with the distance between tags and WiFi RX.

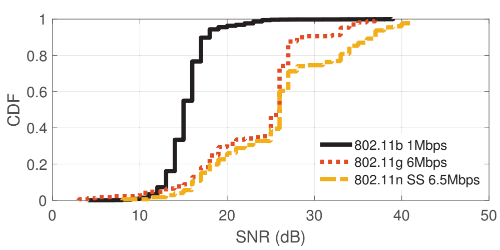

Figure 26: SNR of backscatter signal.

The distance between the WiFi transmitter and the first-hop tag is fixed to 0.3m in all the experiments.

5.2 Communication Ranges

We capture the backscattered packet RSSI information and study how it changes with distances. Since X-Tandem tag supports the identification of different WiFi protocols, we use three types of WiFi excitation signals, including 802.11b DBPSK 1Mbps, 802.11g OFDM BPSK-subcarrier 6Mbps, and 802.11n MIMO-OFDM Single Stream (SS) BPSK-subcarrier 6.5Mbps. The WiFi transmitter generates the excitation signal from Channel 2 (at central frequency 2.417GHz). The WiFi receiver listens on Channel 12 (2.467GHz) for the backscattered signal.

Figure 23 shows how the received backscattered signal RSSI changes with the distance between the X-Tandem second-hop tag and the WiFi receiver in the line-of-sight scenario. In the three subfigures for 802.11b 1Mbps, 802.11g 6Mbps and 802.11n SS 6.5Mbps, the backscattered signal strength shows a general trend of decreasing with tag-to-RX distances. Some points reversing the general downward trend occur in the distance less than 3m. The 802.11g/n backscattered signal strength decreases to less than -80dBm at 3m, and the 802.11b backscattered signal strength decreases to less than -85dBm at 8m.

Figure 24 shows that the communication throughput has a general downward trend when using the three different protocols. The 802.11b backscattered signal achieves up to 200 bits per second throughput when the distance is 0.5m, and the throughput decreases to 50bps at 6.5m. The 802.11g/n signal can achieve up to 60bps throughput with communication ranges up to 3m. Such performance is very limited compared to the single-hop backscatters, e.g., HitchHike [7], which can achieve up to 300Kbps with communication ranges up to 34m. There are two main reasons for this limitation. First, multi-hop path attenuation constrains the tag-to-tag distance and the strength of the last-hop signal that directly impacts the throughput. Second, to reduce decoding complexity, X-Tandem allows each tag to embed information on only a part

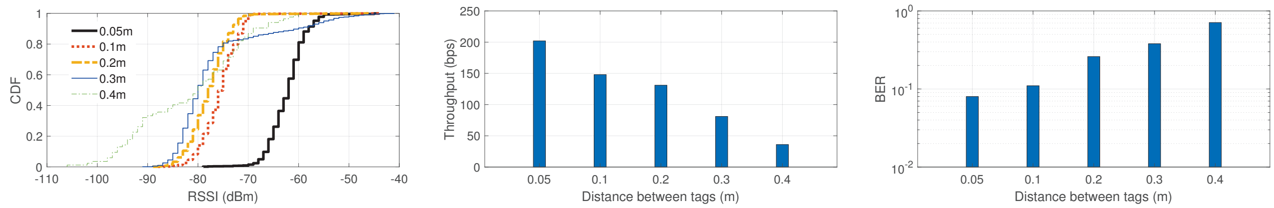

(a) RSSI (b) Throughput (c) Bit error rate

Figure 27: Performance of X-Tandem communication changed with the distance between two tags.

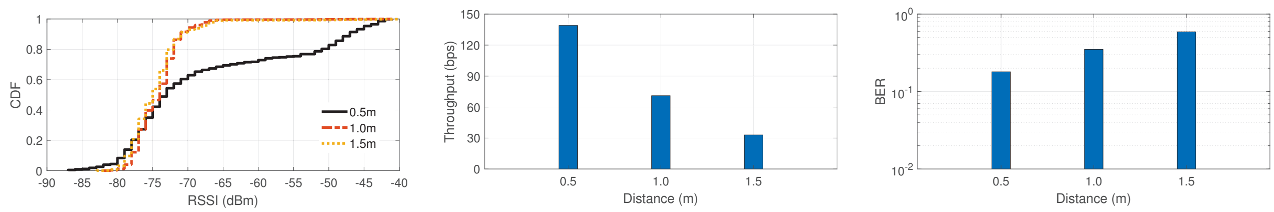

(a) RSSI (b) Throughput (c) Bit error rate

Figure 28: Performance of using tag relay in the experiment scenario of Figure 22(b).

of PPDU data fields, as discussed in Subsection 3.2. We will discuss potential enhancements in Section 8.

Figure 25 shows the decoded tag data BER and how it changes with tag-to-RX distances. For all the three different protocols, the BER values are less than 0.1 when the distance is less than 0.5m. We can see that the BER values generally increase with the tag-to-RX distances in the three subfigures.

In addition to the line-of-sight scenario, we also evaluate X-Tandem in the non-line-of-sight scenario and find that the communication ranges are very limited (less than 0.5m) with weak signal strength (mostly less than -80dBm).

While 802.11b outperforms 802.11g/n in multi-hop backscatter communication ranges, 802.11g/n backscatter signals achieve better SNR than 802.11b at short distance. We use the software tool CommView for WiFi to capture per packet signal level and noise level, from which we can calculate the signal-to-noise ratio (SNR). Figure 26 plots the cumulative distribution function (CDF) of SNR of backscatter signal. The result is measured with a tag-to-RX distance of 0.5m, and it shows that more than 95% of the backscattered 802.11b packets have the SNR in the range from 10dB to 20dB, and more than 50% of the backscattered 802.11g/n packets are within the range from 20dB to 30dB.

5.3 Tag-to-tag Distance

We locate the WiFi receiver two meters away from the first-hop tag. We then move the second-hop tag to increase the distance between the two tags. Figure 27(a) plots the CDF figures of RSSI, corresponding to different tag-to-tag distances. As the distance increases from 0.05m to 0.4m, the backscattered signal strength decreases from more than 70dBm to less than 80dBm. The signal strength decreases very fast from 0.05m to 0.1m. Figure 27(b) and (c) also show that there is a degradation of throughput and BER performance when the tag-to-tag distance increases.

5.4 Obstacles

Figure 22 shows the experiment scenario of using tag relay to increase the communication range. Figure 22(a) is the case of no tag relay, where tag-to-RX communication is severely interfered by the concrete wall. According to our measurement, over 90% packets have signal levels below 85dBm and throughputs below 10 bps with communication ranges within 0.15m. For the case of tag relay in Figure 22(b), the results in Figure 28 shows that the backscattered signal strength is largely increased and the throughput is improved to 135 bps with communication ranges up to 1.5m.

6 APPLICATION CASE

To demonstrate the applicability of X-Tandem in such IoT applications, we have built an indoor environment monitoring system, as illustrated in Figure 29. The system includes an excitation signal source (WiFi sender), a DS18B20 digital thermometer connected to a X-Tandem tag, a DHT11 temperature-humidity sensor connected to another X-Tandem tag, and a sink node (WiFi receiver). DS18B20 and DHT11 collect the temperature and the humidity data and input it as tag bit stream. Via multi-hop backscatter communication, the sensor data is transmitted to the sink node.

We implement the drive circuits of DS18B20 and DHT11 in each tag's FPGA. The data fields of each excitation WiFi

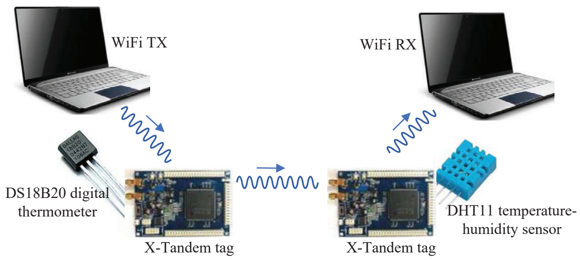

Figure 29: Indoor environment monitoring system using X-Tandem.

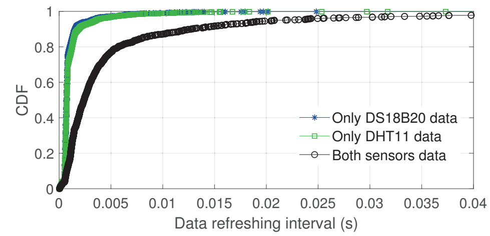

Figure 30: Sensor data refreshing intervals.

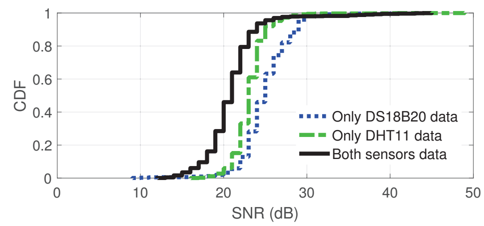

Figure 31: Ratio of signal level to noise level.

packet are set to zeros. The WiFi receiver decodes the sensing data from the backscattered packets. Figure 30 plots the CDF of refreshing intervals of the received sensing data. The interval value is captured from the information of each backscattered packet. The result shows that the case of both tags embedding sensor data has longer packet intervals than the case of using one tag only as a relay. Figure 31 plots the CDF of SNR of the backscattered signal, and it shows that the backscattered signal carrying both sensors data has a lower SNR than the backscattered signal of only one type of sensing data.

7 RELATED WORK

As a low power communication solution, backscatter uses RF reflection mechanisms rather than RF transmitters. Recently, there has been much interest in designing backscatter systems and applying them in diverse sensing applications [2–7, 9–30, 32–36]. More and more IoT applications choose popular wireless communication technologies, such as WiFi and Bluetooth, for their connectivity solutions. This also motivates backscatter systems to be compatible with such commercial radios. Prior work has addressed many compatibility and deployment issues. WiFi Backscatter [2] modulates tag data by changing a WiFi packet's CSI/RSSI information. BackFi [3] designs a backscatter-based IoT sensor that works with WiFi signals. Since then, much effort has been made towards working with off-the-shelf WiFi devices. Passive Wi-Fi [4] uses a backscatter tag infrastructure to significantly reduce the power consumption of WiFi transmissions. The Inter-Technology Backscatter [5] is a backscatter solution that enables communication between WiFi and Bluetooth; FS-Backscatter [6] introduces frequency shifting to achieve a clean WiFi or Bluetooth receiver channel for a backscattered signal; HitchHike [7] proposes a codeword translation approach that enables bit-level tag modulation and decoding with commodity WiFi devices. This approach is further extended to commercial Bluetooth, Zigbee and 802.11g/n WiFi radios [30]. These WiFi-compatible backscatter solutions are all single-hop (transmission from a tag to a reader or AP). Without losing the compatibility (i.e., decoding with off-the-shelf WiFi devices), X-Tandem enables multi-hop backscatter communication, which is different from the previous single-hop systems.

A backscatter tag can also be designed for decoding. Prior work on Ambient Backscatter [16] designs a decoding-enabled tag and it allows two battery-free tags to communicate by backscattering ambient RF signals. Specifically, an Ambient Backscatter tag uses analog hardware to digitally decode the incoming information from other tags. X-Tandem differs from the design of Ambient Backscatter in the following aspects. First, X-Tandem is a multi-hop backscatter system that enables tag relay using analog forwarding with decoding-free tags (i.e., a tag can simply forward the analog signals from previous hops without decoding these signals). The current implementation of X-Tandem does not involve tag-to-tag communication, thus reducing the need of the tag hardware for decoding. Second, X-Tandem performs multi-hop tag modulation in a single packet, which requires each tag to do relay and modulation simultaneously. An Ambient Backscatter tag however does not forward other tags information. Furthermore, X-Tandem works with WiFi signals, while Ambient Backscatter works with TV or cellular signals.

Limited communication range is a major concern of RFID infrastructures. Recent work on RFly [31] uses drones as relay between an RFID tag and a reader in both line-of-sight and non-line-of-sight environments. RFly drones are equipped with a customized relay system that can localize RFID tags and forward a reader's query to a tag or forward the tag's reply to the reader. X-Tandem differs from RFly in three ways. First, RFly is an external relay device added to an already deployed RFID infrastructure, while X-Tandem enables a backscatter system itself to be capable of doing relays (i.e., a tag by itself can forward other tags information). Second, RFly relays without generating any data of its own, while each X-Tandem tag conveys its own information simultaneously with doing relays. Third, RFly works with RFID infrastructures, while X-Tandem is compatible with commodity WiFi and is easy to extend its function by connecting diverse off-the-shelf sensors to the tag hardware.

8 DISCUSSION AND CONCLUSION

For a sequence of backscattering that involves the original excitor and a series of N backscatters, refer to the i-th backscatter that processes and reflects the signal as Backscatter(i) or $B(i)$ for simplicity, and the reflected signal as the i-th order signal, or $S(i)$. Existing backscatter communication systems are typically of order 1, and our X-Tandem represents the first effort towards higher order backscattering. It opens the door from *backscatter communication* to *backscatter networking*, which we believe will serve as a foundation for the future battery-less passive Internet of Things. Many applications can be built on top of this more scalable, flexible, and robust networked systems with ultra-low-power and ultra-small-form-factor devices.

Our preliminary implementation demonstrates that a 2nd order backscatter system can be deployed with state-of-the-art commodity WiFi devices. The existence of one relay can already avoid many of the obstacles in realworld, thereby significant improving the applicability of backscatter communication. Our design is not restricted to 2nd order only; moving toward even higher order, however, faces a series of challenges, which we discuss as below.

Signal attenuation by analog forwarding. RF signal power attenuates significantly after multiple times of reflection, i.e., $S(i)$ can be too weak to be useful when $i > 2$. Although the MFS scheme in X-Tandem eliminates the inference among $S(i)$s, it uses analog forwarding by reflecting the excitation signal multiple times and thus faces the issue of signal attenuation. Only the last-hop backscattered signal is used for decoding, and its strength limits the number of tags, tag-to-tag distances, and communication ranges. Potential enhancements include: (i) enabling a tag to first decode and then forward the previous hops information, so that the tag can directly backscatter excitation signals; and (ii) using long-range communication techniques, e.g., LoRa [33, 34], to improve communication range.

Dynamic frequency shift and receive channel setting. Although X-Tandem can control tags to work in either the relay mode or the non-relay mode, the frequency shift implementation in each tag is static (25MHz), which is unable to adapt to ongoing transmission conditions. For example, unreliable channel state may degrade X-Tandem's performance, which will be even worse when multiple groups of tag-relay communications collide due to the lack of MAC mechanisms. Dynamic frequency shift needs hardware modification, such as channel quality detection circuits, extra oscillators, and FPGA internal circuits with multiple input clocks or single input clock multiple frequency division. The receive channel is also fixed at channel 12 in our implementation. Adaptive receive channel needs software modification for decoding, as well as extra control signals coordinating tag and RX for channel selection.

Fixed routing vs. dynamic routing. Subsection 3.5 uses an RSSI-based packet verification scheme to eliminate the out-of-order backscattered packets that contradict the route order set by the control signals. While X-Tandem has flexibility to set the order of multi-hop backscattering for tags, the routing is fixed after the tags receive the related control signals. This design is necessary for the static deployment, but may face challenges in the situations where tags work with portable sensors or mobile devices. A possible solution for dynamic routing is to use the control signals to update the hop order timely according to the TX-to-tag distances and tag-to-RX distances. Backscatter-based localization technologies [42, 43] would be helpful for such design goals.

Limited throughput. The experiment results show that X-Tandem achieves up to 200 bps throughput for $S(2)$, which is very limited compared to $S(1)$ with state-of-art implementations. Although this throughput works for simple applications as sensor data reading (see our case study), it is well below the expectation for streaming media data, not to mention AR/VR data. An X-Tandem tag uses a part of the data fields for modulation rather than the whole data fields of a packet. This mechanism reduces the BER and the deployment complexity, yet sacrificing per tag throughput. The tradeoff, as we have discussed in Subsection 3.2, is that if the modulation uses multiple times of phase change on the whole data fields, per tag throughput will increase but bit errors and decoding complexity would also increase.

Advanced features in the latest WiFi standards, i.e., 802.11ac and beyond, may be explored to further boost the throughput. Given the recent success of backscattering HD video signals [36] and spatial stream backscattering with advanced OFDM WiFi devices [30, 37], such challenging applications as AR/VR streaming over backscatter networks can also be envisioned, if not instantly available, saving users from wearing bulky lens or helmets with short-lived batteries.

ACKNOWLEDGMENTS

We would like to thank the anonymous shepherd and reviewers for their valuable and insightful comments. This work was supported by a Canada Technology Demonstration Program (TDP) grant, a Canada NSERC Discovery Grant, an NSERC E.W.R. Steacie Memorial Fellowship, and Key Research Program of Frontier Sciences, CAS, No. QYZDY-SSW-JSC002. Contact author: Jiangchuan Liu (jcliu@sfu.ca).

REFERENCES

[1] S. Gollakota, M. S. Reynolds, J. R. Smith, and D. J. Wetherall. The Emergence of RF-Powered Computing. *Computer*, 47(1): 32-39, 2014.

[2] B. Kellogg, A. Parks, S. Gollakota, J. R. Smith, and D. Wetherall. WiFi Backscatter: Internet Connectivity for RF-Powered Devices. *ACM SIGCOMM*, 2014.

[3] D. Bharadia, K. Joshi, M. Kotaru, and S. Katti. BackFi: High Throughput WiFi Backscatter. *ACM SIGCOMM*, 2015.

[4] B. Kellogg, V. Talla, S. Gollakota, and J. R. Smith. Passive Wi-Fi: Bringing Low Power to Wi-Fi Transmissions. *USENIX NSDI*, 2016.

[5] V. Iyer, V. Talla, B. Kellogg, S. Gollakota, and J. R. Smith. Inter-Technology Backscatter: Towards Internet Connectivity for Implanted Devices. *ACM SIGCOMM*, 2016.

[6] P. Zhang, M. Rostami, P. Hu, and D. Ganesan. Enabling Practical Backscatter Communication for On-body Sensors. *ACM SIGCOMM*, 2016.

[7] P. Zhang, D. Bharadia, K. Joshi, and S. Katti. HitchHike: Practical Backscatter Using Commodity WiFi. *ACM SenSys*, 2016.

[8] J. -P. Curty, N. Joehl, F. Krummenacher, C. Dehollain, and M. J. Declercq. Model for μ-Power Rectifier Analysis and Design. *IEEE Trans. Circuits and Systems*, 52(12): 2771-2779, 2005.

[9] O. Abari, D. Vasisht, D. Katabi, and A. Chandrakasan. Caraoke: An E-Toll Transponder Network for Smart Cities. *ACM SIGCOMM*, 2015.

[10] J. Gummeson, P. Zhang, and D. Ganesan. Flit: A Bulk Transmission Protocol for RFID-Scale Sensors. *ACM MobiSys*, 2012.

[11] H. Hassanieh, J. Wang, D. Katabi, and T. Kohno. Securing RFIDs by Randomizing the Modulation and Channel. *USENIX NSDI*, 2015.

[12] P. Hu, P. Zhang, and D. Ganesan. Leveraging Interleaved Signal Edges for Concurrent Backscatter. *ACM HotWireless*, 2014.

[13] P. Hu, P. Zhang, and D. Ganesan. Laissez-faire: Fully Asymmetric Backscatter Communication. *ACM SIGCOMM*, 2015.

[14] P. Hu, P. Zhang, M. Rostami, and D. Ganesan. Braidio: An Integrated Active-Passive Radio for Mobile Devices with Asymmetric Energy Budgets. *ACM SIGCOMM*, 2016.

[15] B. Kellogg, V. Talla, and S. Gollakota. Bringing Gesture Recognition to All Devices. *USENIX NSDI*, 2014.

[16] V. Liu, A. Parks, V. Talla, S. Gollakota, D. Wetherall, and J. R. Smith. Ambient Backscatter: Wireless Communication Out of Thin Air. *ACM SIGCOMM*, 2013.

[17] V. Liu, V. Talla, and S. Gollakota. Enabling Instantaneous Feedback with Full-Duplex Backscatter. *ACM MobiCom*, 2014.

[18] A. N. Parks, A. Liu, S. Gollakota, and J. R. Smith. Turbocharging Ambient Backscatter Communication. *ACM SIGCOMM*, 2014.

[19] V. Talla, B. Kellogg, B. Ransford, S. Naderiparizi, S. Gollakota, and J. R. Smith. Powering the Next Billion Devices with Wi-Fi. *ACM CoNEXT*, 2015.

[20] J. Wang, F. Adib, R. Knepper, D. Katabi, and D. Rus. RF-Compass: Robot Object Manipulation Using RFID. *ACM MobiCom*, 2013.

[21] J. Wang, H. Hassanieh, D. Katabi, and P. Indyk. Efficient and Reliable Low-Power Backscatter Networks. *ACM SIGCOMM*, 2012.

[22] J. Wang and D. Katabi. Dude, Where's My Card?: RFID Positioning That Works with Multipath and Non-Line of Sight. *ACM SIGCOMM*, 2013.

[23] J. Wang, D. Vasisht, and D. Katabi. Rf-idraw: Virtual Touch Screen in the Air Using RF Signals. *ACM SIGCOMM*, 2014.

[24] P. Zhang and D. Ganesan. Enabling Bit-by-Bit Backscatter Communication in Severe Energy Harvesting Environments. *USENIX NSDI*, 2014.

[25] P. Zhang, D. Ganesan, and B. Lu. Quarkos: Pushing the Operating Limits of Micro-Powered Sensors. *USENIX HotOS*, 2014.

[26] P. Zhang, J. Gummeson, and D. Ganesan. Blink: A High Throughput Link Layer for Backscatter Communication. *ACM MobiSys*, 2012.

[27] P. Zhang, P. Hu, V. Pasikanti, and D. Ganesan. Ekhonet: High Speed Ultra Low-Power Backscatter for Next Generation Sensors. *ACM MobiCom*, 2014.

[28] A. Wang, V. Iyer, V. Talla, J. R. Smith, and S. Gollakota. FM Backscatter: Enabling Connected Cities and Smart Fabrics. *USENIX NSDI*, 2017.

[29] V. Talla, B. Kellogg, S. Gollakota, and J. R. Smith. Battery-free Cellphone. *ACM UbiComp*, 2017.

[30] P. Zhang, C. Josephson, D. Bharadia, and S. Katti. FreeRider: Backscatter Communication Using Commodity Radios. *ACM CoNEXT*, 2017.

[31] Y. Ma, N. Selby, and F. Adib. Drone Relays for Battery-Free Networks. *ACM SIGCOMM*, 2017.

[32] X. Xu, Y. Shen, J. Yang, C. Xu, G. Shen, G. Chen, and Y. Ni. PassiveVLC: Enabling Practical Visible Light Backscatter Communication for Battery-free IoT Applications. *ACM MobiCom*, 2017.

[33] V. Talla, M. Hassar, B. Kellogg, A. Najafi, J. Smith, and S. Gollakota. LoRa Backscatter: Enabling the Vision of Ubiquitous Connectivity. *ACM Ubicomp*, 2017.

[34] Y. Peng, L. Shangguan, Y. Hu, Y. Qian, X. Lin, X. Chen, D. Fang, and K. Jamieson. PLoRa: Passive Long-Range Data Networks from Ambient LoRa Transmissions. *ACM SIGCOMM*, 2018.

[35] D. Vasisht, G. Zhang, O. Abari, D. Katabi, H. -M. Lu, and J. Flanz. In-body Backscatter Communication and Localization. *ACM SIGCOMM*, 2018.

[36] S. Naderiparizi, M. Hessar, V. Talla, S. Gollakota, and J. R. Smith. Towards Battery-Free HD Video Streaming. *USENIX NSDI*, 2018.

[37] J. Zhao, W. Gong, and J. Liu. Spatial Stream Backscatter Using Commodity WiFi. *ACM MobiSys*, 2018.

[38] O. Gnawali, R. Fonseca, K. Jamieson, D. Moss, and P. Levis. Collection Tree Protocol. *ACM SenSys*, 2009.

[39] C. Raiciu, S. Barre, C. Pluntke, A. Greenhalgh, D. Wischik, and M. Handley. Improving Datacenter Performance and Robustness with Multipath TCP. *ACM SIGCOMM*, 2011.

[40] J. Zhao, J. Liu, H. Wang, and C. Xu. Multipath TCP for Datacenters: From Energy Efficiency Perspective. *IEEE INFOCOM*, 2017.

[41] L. Li, K. Xu, T. Li, K. Zheng, C. Peng, D. Wang, X. Wang, M. Shen, and R. Mijumbi. A Measurement Study on Multi-path TCP with Multiple Cellular Carriers on High-speed Rails. *ACM SIGCOMM*, 2018.

[42] M. Kotaru, P. Zhang, and S. Katti. Localizing Low-power Backscatter Tags Using Commodity WiFi. *ACM CoNEXT*, 2017.

[43] L. Yang, Y. Chen, X. Li, C. Xiao, Mo Li, and Y. Liu. Tagoram: Real-Time Tracking of Mobile RFID Tags to High Precision Using COTS Devices. *ACM MobiCom*, 2014.

[44] IEEE Std 802.11-1999. Wireless LAN Medium Access Control (MAC) and Physical Layer (PHY) specifications.

[45] IEEE Std 802.11a-1999. Wireless LAN Medium Access Control (MAC) and Physical Layer (PHY) specifications: High-speed Physical Layer in the 5 GHZ Band.

[46] IEEE Std 802.11g-2003. Wireless LAN Medium Access Control (MAC) and Physical Layer (PHY) specifications, Amendment 4: Further Higher Data Rate Extension in the 2.4 GHz Band.

[47] IEEE Std 802.11n-2009. Wireless LAN Medium Access Control (MAC) and Physical Layer (PHY) specifications, Amendment 5: Enhancements for Higher Throughput.